A comprehensive study of g-factors, elastic, structural and electronic properties of III-V semiconductors using hybrid-density functional theory

Carlos M. O. Bastos, Fernando P. Sabino, Guilherme M. Sipahi, and Juarez L. F. Da Silva

Citation: Journal of Applied Physics **123**, 065702 (2018);
View online: https://doi.org/10.1063/1.5018325
View Table of Contents: http://aip.scitation.org/toc/jap/123/6
Published by the American Institute of Physics

A comprehensive study of *g*-factors, elastic, structural and electronic properties of III-V semiconductors using hybrid-density functional theory

Carlos M. O. Bastos,[1] Fernando P. Sabino,[1] Guilherme M. Sipahi,[1] and Juarez L. F. Da Silva[2,a)]
[1]*São Carlos Institute of Physics, University of São Paulo, PO Box 369, 13560-970 São Carlos, SP, Brazil*
[2]*São Carlos Institute of Chemistry, University of São Paulo, PO Box 780, 13560-970 São Carlos, SP, Brazil*

(Received 5 December 2017; accepted 18 January 2018; published online 9 February 2018)

Despite the large number of theoretical III-V semiconductor studies reported every year, our atomistic understanding is still limited. The limitations of the theoretical approaches to yield accurate structural and electronic properties on an equal footing, is due to the unphysical self-interaction problem that mainly affects the band gap and spin-orbit splitting (SOC) in semiconductors and, in particular, III-V systems with similar magnitude of the band gap and SOC. In this work, we report a consistent study of the structural and electronic properties of the III-V semiconductors by using the screening hybrid-density functional theory framework, by fitting the α parameters for 12 different III-V compounds, namely, AlN, AlP, AlAs, AlSb, GaN, GaP, GaAs, GaSb, InN, InP, InAs, and InSb, to minimize the deviation between the theoretical and experimental values of the band gap and SOC. Structural relaxation effects were also included. Except for AlP, whose $\alpha = 0.127$, we obtained α values that ranged from 0.209 to 0.343, which deviate by less than 0.1 from the universal value of 0.25. Our results for the lattice parameter and elastic constants indicate that the fitting of α does not affect those structural parameters when compared with the HSE06 functional, where $\alpha = 0.25$. Our analysis of the band structure based on the $\mathbf{k} \cdot p$ method shows that the effective masses are in agreement with the experimental values, which can be attributed to the simultaneous fitting of the band gap and SOC. Also, we estimate the values of *g*-factors, extracted directly from the band structure, which are close to experimental results, which indicate that the obtained band structure produced a realistic set of $\mathbf{k} \cdot p$ parameters. *Published by AIP Publishing.*
https://doi.org/10.1063/1.5018325

I. INTRODUCTION

Semiconductors have been playing a key role in the development of new technologies since the 1950s, e.g., light-emitting diodes and lasers,[1–3] infrared detectors,[4] solar cells,[5] and, more recently, spin-lasers.[6] These developments have been possible due to the large number of fundamental studies that used theoretical or experimental techniques, along the decades,[7,8] which have contributed to the present understanding of the semiconductors electronic band-structure properties, punctual and extended defects, and structural control.[8,9] Beyond that, new fields have emerged along the years, such as topological insulators[10] and Majorana fermions in nanowires,[11,12] which are expected to contribute to future technological applications.

Among a wide range of semiconductor materials,[7–9,13] the III-V *AB* semiconductors, where $A =$ Al, Ga, In, and where $B =$ N, P, As, Sb (i.e., 12 compounds), occupy an important place due to their role in several technological developments.[1,2,4–6] Although there is an impressive number of papers published every year based on experimental and/or first-principles calculations,[3,14–20] our atomistic understanding is still limited, in particular, due to the limitations in theoretical approaches to describe structural and electronic properties on an equal footing. For example, first-principles calculations based on density functional theory (DFT), with local or semilocal exchange-correlation energy functionals, have the unphysical self-interaction problem,[21–23] which mainly affects the band gap and spin-orbit splitting (SOC) in semiconductors,[22,24] and, in particular, for a few III-V *AB* semiconductors, where the SOC can have a similar magnitude as the band gap, e.g., GaSb, InP, InAs, and InSb.[9,25]

Along the years, the self-interaction problem has motivated the widespread use of approximations or alternative descriptions of the electronic states, such as the GW[26,27] or the nonlocal hybrid density functionals, e.g., PBE0,[28,29] HSE06,[30–32] and B3LYP.[33] In principle, both GW and hybrid-DFT can yield an improved description of the band structure compared with local or semilocal functionals; however, GW was designed to address electronic properties but not the structural properties.[26,27] In contrast with GW, hybrid-DFT can describe both structural and electronic properties on an equal footing; however, the electronic properties, e.g., the band gap, depend strongly on the magnitude of the nonlocal Fock exchange, α, that replaces part of the semilocal exchange term. Although a universal value for α was suggested, i.e., 25% in PBE0,[28,30] it is not as universal as expected.[34]

Because the band increases almost linearly by increasing the magnitude of the nonlocal Fock exchange,[35] several studies proposed a fitting of the α parameter to improve the description of the band gap.[34–36] However, those studies

a)Author to whom correspondence should be addressed: juarez_dasilva@iqsc.usp.br

used, in most cases, atomic structures optimized with the local or semilocal functionals,[37–39] i.e., the differences in the structural parameters, are neglected. This is a good approximation, but it might fail in cases in which the fine details of the electronic structure strongly depend on the lattice parameters, e.g., III-V systems with large SOC.

In this work, we propose to perform a consistent study of the structural and electronic properties of the III-V semiconductors by using the screening hybrid-DFT framework, where the α parameters for the different compounds are fitted by the minimization of the deviation between the theoretical and experimental values for the band gap and SOC. We also used optimized lattice parameters based on screening hybrid-DFT, i.e., small differences in the lattice constant were taken into account for the electronic parameters. Based on this framework, we calculated the equilibrium lattice constant, elastic constants, bulk modulus, band structures, effective masses, etc. Furthermore, we used the $\mathbf{k}\cdot p$ method to perform a deep analysis of the band structures, from which it was possible to extract the $\mathbf{k}\cdot p$ parameters and the electronic g-factors.

Except for AlP, we obtained α parameters, which ranged from 0.209 to 0.343, i.e., close to the universal value of 0.25. For AlP, the calculated α value is 0.127. Based on several analyses, we found, with few exceptions, that the α values correlate well with the atomic radius of the cationic species, and, hence, α values for different semiconductors could be extrapolated from this finding without additional calculations. Our results for the lattice and elastic constants indicate that the fitting of the α does not affect those structural parameters when compared with the HSE06 functional, where $\alpha = 0.25$.

Our analysis of the band structure based on the $\mathbf{k}\cdot p$ method shows that the effective masses are in agreement with the experimental values,[9,40] i.e., the fitting of α at the Γ point improved the description of the band curvatures. We also determined the g-factors directly from the effective band structures and found values that are close to the experimental results.[9,25] Finally, with having both g-factors and effective masses in good agreement with the experimental results indicates that we determined realistic sets of $\mathbf{k}\cdot p$ parameters.

II. THEORETICAL APPROACH AND COMPUTATIONAL DETAILS

A. Density functional theory

It has been known for decades that DFT[41,42] within local (local density approximation—LDA)[43] or semilocal (generalized gradient approximation—GGA)[44,45] exchange-correlation energy functionals is unable to yield a correct description of the fundamental band gap even for the most simple systems,[22,24] which has mainly been attributed to the unphysical self-interaction problem.[21–23] This limitation has motivated the widespread use of approximations or alternative descriptions of the electronic valence states, such as the GW[26,27] or nonlocal hybrid functional, e.g., PBE0,[29,46] HSE06,[30–32] and B3LYP.[33] In principle, both the GW and nonlocal hybrid functionals can yield an improved description of the band structure compared with LDA or GGA. However, in contrast with the GW framework, the nonlocal hybrid functional can also provide a reliable description of the structural and energetics properties,[39,47–49] which is a plus compared with GW.

In this work, we use the DFT framework within the GGA formulation proposed by Perdew, Burk, and Ernzerhof[45] (PBE) and the hybrid functional proposed by Heyd, Scuzeria, and Ernzerhof[30–32] (HSE), in which the magnitude of the nonlocal Fock exchange replaces part of the PBE exchange. As will be described below, we fit the magnitude of the nonlocal Fock exchange based on the experimental results of the fundamental band gap and the spin-orbit (SO) splitting, while using the same screening parameter derived for the HSE06 functional.[32,50]

To describe the electronic states we used the scalar-relativistic approximation[51,52] in which relativistic corrections are considered for the core-states, whereas the SOC is not considered for the valence states, and hence, the spin-orbit splitting for the III-V semiconductors cannot be described. For example, for InSb, the SOC splitting at the Γ-point and valence band maximum (VBM) has a similar magnitude as the fundamental band gap,[24,53] and, hence, it plays a crucial role for the characterization of the band structure parameters, e.g., effective mass, g-factor. Thus, to improve the description of the band structure properties, we used the addition of the SOC for the valence states via the second-variational approach.[51]

To solve the Kohn–Sham equations, we used the projected augmented wave (PAW) method,[54] as implemented in the Vienna *ab initio* simulation package (VASP, version 5.4.1)[55,56] by using the PAW projectors provided with the package.[57] To describe the electronic states, the Kohn–Sham orbitals are expanded in plane waves by using a finite cutoff energy, which depends on the calculated properties. This is necessary because several properties, e.g., stress tensor and elastic constants, converge slowly as the number of plane waves increases.

From a large number of PBE and HSE convergence tests, we demonstrated that well-converged total energies, band structures, and densities of states can be obtained by using a cutoff energy that is 1.125 times the recommended maximum cutoff energy ($\mathrm{ENMAX_{max}}$). Stress tensor and elastic constants calculations, however, require at least $1.50 \times \mathrm{ENMAX_{max.}}$ A further increase in the cutoff energy can slightly improve the results, and, for the particular case of the PBE calculations, we increased the multiplication factor from 1.50 to 2.0 (stress tensor) and to 2.5 (elastic constants) in aiming to provide reference data that can be used for further comparisons. For example, for AlN, we used 473 eV for total energy and band structure, 631 eV (HSE) and 841 eV (PBE) for stress tensor, and 631 eV (HSE) and 1052 eV (PBE) for the elastic constants calculations. For the Brillouin zone integration, we used a Monkhorst–Pack $\mathbf{k}$-mesh of $10 \times 10 \times 10$, whereas the same $\mathbf{k}$-point density was used for the remaining III-V semiconductors. All these parameters are provided in the supplementary material.

To obtain the equilibrium volume, we minimized the stress tensor, which was performed by several consecutive

optimizations of the equilibrium volume to ensure that the optimized equilibrium volume is consistent with the initial setup of the basis vector sizes. To calculate the elastic properties, we considered the combination of two schemes, namely, (i) rigid lattice parameters obtained from the stress-tensor optimization[58] and (ii) ionic volume relaxation from the inversion of the ionic Hessian matrix and internal stress tensor,[59] as implemented in VASP. For those calculations, we used atomic steps of 0.010 Å, which are slightly smaller than the recommended value by VASP, e.g., 0.15 Å.

B. Hybrid HSE functional: Fitting of the α value

The hybrid PBE0 functional is composed of the PBE correlation energy, and a fraction of 25% of the PBE exchange is replaced by the nonlocal Fock exchange of the Hartree–Fock (HF) method, i.e., $E_{XC}^{PBE0} = E_c^{PBE} + \alpha E_x^{HF} + (1-\alpha)E_x^{PBE}$, where $\alpha = 0.25$.[29,46] The hybrid HSE functional[30–32] is derived from PBE0 by using a screening function to split the semilocal PBE exchange and nonlocal Fock term into two parts, namely, short- (SR) and long-range (LR) exchange contributions, in which the nonlocal Fock LR contribution cancels with part of the PBE LR exchange. Thus, the hybrid HSE functional is given by the following equation:

$$E_{XC}^{HSE} = E_c^{PBE} + E_x^{PBE,LR}(\omega) + \alpha E_x^{HF,SR}(\omega) + (1-\alpha)E_x^{PBE,SR}(\omega), \quad (1)$$

where the new parameter, ω, measures the intensity of the screening and, hence, the extension of the nonlocal Fock interactions. For example, if ω is null, then the SR contribution is equivalent to the full Fock operator and the LR contribution will become zero, whereas for $\omega \to \infty$, the range of SR terms decrease, which asymptotically recovered the PBE functional. As defined in the PBE0 functional, the parameter α controls the amount of PBE exchange replaced by the nonlocal Fock exchange, and, hence, in principle, it can range from 0 to 1. For the hybrid HSE06 functional, $\alpha = 0.25$ was obtained from the adiabatic perturbation theory and $\omega = 0.206\ \text{Å}^{-1}$ was fitted using a large number of systems, respectively.[32,50]

Although, the hybrid HSE06 functional yields better results than the LDA and GGA functionals, HSE06 does not yield the experimental band gaps in most of the cases,[24,60,61] and, hence, improved results can be obtained by fitting the ω or α parameters. Recently, Viñes *et al.*[34] indicated that a large number of combinations of ω and α values can yield the band gap of oxides; however, it is important to mention that the fitting of ω can drastically affect the small contribution of the LR nonlocal Fock terms, which has the potential to decrease the stability of the electron density convergence. In contrast with ω, the fitting of α mainly affects the SR nonlocal Fock contribution, which plays a crucial role in the physical properties.[62–65]

Therefore, to improve the description of the experimental fundamental band gap, E_{gap}, and the spin-orbit (SO) splitting energies, Δ_{so}, we fixed the ω parameter to the same value used in HSE06 and fitted the α parameter to reproduce the experimental E_{gap} and Δ_{so} results. The fitting was performed by using the linear dependence of E_{gap} and Δ_{so} as a function of α, which is well known in the literature.[66–68] Due to the nearly perfect linear dependence, the angular coefficient (slope) can be calculated by using two points, namely, by using the E_{gap} or $E_{\Delta_{so}}$ values calculated with the PBE ($\alpha = 0$) and HSE06 ($\alpha = 0.25$) functionals. Thus, the angular coefficient for the fitting of the band gap is given by the following relation:

$$m_{gap} = \frac{E_{gap}^{HSE06} - E_{gap}^{PBE}}{0.25}, \quad (2)$$

while $m_{\Delta_{so}}$ is obtained by replacing the band gap energies by the spin-orbit splittings. Thus, the α value that yields the experimental band gap, E_{gap}^{exp}, or the experimental spin-orbit splitting, $E_{\Delta_{so}}^{exp}$, can be obtained from the following equation:

$$\alpha_{gap} = \frac{E_{gap}^{exp} - E_{gap}^{PBE}}{m_{gap}}. \quad (3)$$

Consequently, from this scheme, we obtained two values for α, namely, an optimized value for α_{gap} ($\alpha_{\Delta_{so}}$) that yields the experimental band gap (spin-orbit splitting). To obtain a unique α for each III-V system, we performed a minimization of the standard deviation between the experimental and the extrapolated E_{gap}^{exp} and $E_{\Delta_{so}}^{exp}$ parameters obtained from the slope. Further technical details are reported in the supplementary material. Thus, from now on, the fitted hybrid HSE functional is noted as HSE_{α}, where α is different for each semiconductor. Finally, to compare our results with the literature and among different functionals, we adopted, as a measure, the normalized-root-mean-square deviation (NRMSD).[69]

III. RESULTS

A. Magnitude of the non-local Fock exchange

Except for AlP, the optimal α values that minimize the relative errors for the fundamental band gap and SOC splitting are in between 0.209 and 0.343, i.e., close to the universal value of 0.25.[28] For AlP, the value is 0.127. Therefore, we conclude that a unique α value is unable to yield the fundamental band gap and SOC splitting for a wide range of compounds as well as further physical properties, which have also been reported in a previous study.[66] Although the value of α has been obtained from a solid theoretical framework, to our knowledge only one study has tried to obtain a correlation between the magnitude of α and a particular physical property,[34] which can help in several applications. Thus, with the aim to identify the most important physical parameters that play major roles in the magnitude of α, we performed several analyses (also in the supplementary material). Among all analyses, we found a good correlation between the magnitude of α versus the cationic radius,[70] which is shown in Fig. 1. Our results indicate that the value of the optimized α decreases almost linearly as a function of the atomic cationic radius, except for the cases of AlN and AlP.

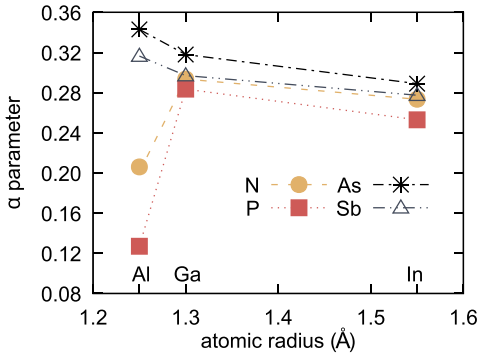

FIG. 1. Optimal magnitude of the nonlocal Fock exchange, α, in the hybrid HSE$_\alpha$ functional obtained from the fitting of the fundamental band gap and the spin-orbit coupling versus the cation atomic radii obtained from Ref. 70. The atomic radii are given in Å and α is dimensionless.

B. Equilibrium lattice parameter

The most stable crystalline phase of the III-V semiconductors is the zinc-blende structure,[71] which has a face-centered cubic (fcc) lattice and $F\bar{4}3m$ space group. The exceptions for this rule are the III-nitrides (AlN, GaN, InN), which prefer to crystallize in the hexagonal wurtzite structure, which belongs to the $P6_3mc$ space group;[72] however, through the use of experimental techniques such as molecular beam epitaxy, they can also be grown as a zinc-blende structure.[7,72] Thus, to rationalize our understanding, all the III-V semiconductors were studied in the zinc-blende structure, which contains two fourfold atoms with tetrahedral local symmetry. The equilibrium lattice parameter, a_0, was calculated by using several approximations, namely, PBE, PBE+SOC, HSE06, and HSE$_\alpha$, and the results are summarized in Table I, along with the experimental results.

In agreement with previous DFT-PBE calculations,[38,60,75] we obtained equilibrium PBE lattice constants that overestimate experimental results, with the largest deviation smaller than 2.2% for InSb. The addition of the SOC for the valence states reduces the lattice constant only to the third decimal place, and, hence, the improvement over the PBE compared with the experimental results is almost negligible and can be evaluated by the NRMSD, shown in Table I. For example, the NRMSD is 1.49% for PBE and 1.47% for PBE+SOC. Therefore, the SOC does not affect the equilibrium lattice constants, in contrast with the electronic properties, where it plays an essential role (see below).

To reduce the computational cost, which increases substantially for HSE06+SOC, the HSE06 and HSE$_\alpha$ equilibrium lattice constants were calculated by using stress tensor without the addition of the SOC for the valence states. The HSE06 and HSE$_\alpha$ functionals yield a_0 parameters closer to the experimental results and, hence, with smaller relative errors compared with the PBE results. These small errors were expected because we provided an improved description of the exchange energy by the nonlocal Fock term. The differences between the HSE06 and HSE$_\alpha$ results are very small, i.e., the NRMSD changes from 0.4% (HSE06) to 0.49% (HSE$_\alpha$). This is an important result because it shows that the lattice parameters were only slightly affected by the improvement of the description of the fundamental band gap and spin-orbit splitting at the Γ-point. The HSE06 results are in excellent agreement with previous hybrid HSE06 results,[61] e.g., indium composites have differences smaller than 0.3%, 0.4%, and 0.5% for InP, InAs, and IsnSb, respectively.

The lattice parameter has a slight linear dependence with the atomic radius of the material compound elements (occupation of the electronic shells), i.e., if the anionic atom size increases, then the lattice parameter also increases, as shown in Fig. 2. This effect occurs due to the electrostatic repulsion between atoms, i.e., the bond length depends on the atom size by changing the lattice parameter. Because Al and Ga have similar atomic radii, with 1.25 Å and 1.30 Å, respectively,[70] the lattice parameters for the Al-V compounds are closer to the Ga-V values, as shown in Fig. 2. The In has a greater atomic radius, 1.55 Å,[70] which results in a larger lattice parameter for the In-V compounds. To

TABLE I. Equilibrium lattice parameters a_0 (in Å) for all the III-V semiconductors, calculated with the PBE, PBE with spin-orbit coupling for the valence states (PBE+SOC), HSE06, and HSE$_\alpha$ functionals. For the hybrid HSE$_\alpha$ functional, the adjusted α parameter is indicated within parentheses. The NRMSD indicates the normalized percentage deviation between theoretical and experimental parameters for the full series.

	PBE	PBE+SOC	HSE06	HSE$_\alpha$ (α)	Exp.
AlN	4.399	4.399	4.361	4.367 (0.219)	4.38[a]
AlP	5.505	5.505	5.471	5.487 (0.127)	5.46[b]
AlAs	5.731	5.731	5.678	5.660 (0.343)	5.661[b]
AlSb	6.213	6.215	6.160	6.146 (0.318)	6.135[b]
GaN	4.545	4.545	4.492	4.483 (0.293)	4.52[a]
GaP	5.499	5.499	5.456	5.449 (0.283)	5.45[b]
GaAs	5.742	5.738	5.669	5.652 (0.318)	5.653[b]
GaSb	6.203	6.203	6.124	6.124 (0.297)	6.095[b]
InN	5.042	5.039	4.976	4.956 (0.274)	4.97[c]
InP	5.946	5.942	5.886	5.885 (0.253)	5.868[b]
InAs	6.174	6.172	6.090	6.078 (0.289)	6.058[b]
InSb	6.619	6.618	6.526	6.549 (0.277)	6.479[b]
NRMSD	1.49	1.47	0.40	0.49	…

[a]From Ref. 73.
[b]From Ref. 9.
[c]From Ref. 74.

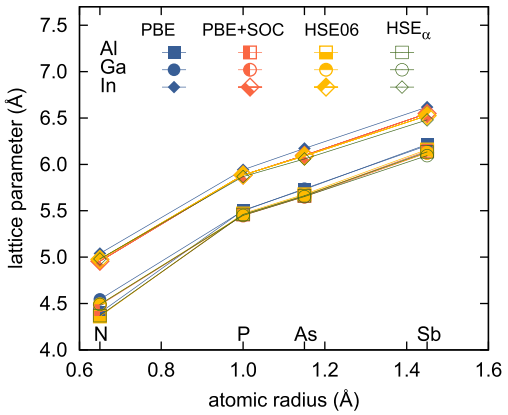

FIG. 2. Lattice parameters versus the atomic radius of the anion species. The lattice parameters were obtained by using the following exchange-correlation functionals: PBE, PBE+SOC, HSE06, HSE$_\alpha$. The atomic radii were extracted from Ref. 70.

TABLE II. Elastic constants calculated with PBE and α-optimized HSE (HSE_α), functionals. The bulk moduli, B_0, were obtained from the elastic constants results, namely, $B_0 = (C_{11} + 2C_{12})/3$, and are compared with the experimental values obtained from elastic constants ($Exp.^{C_{ij}}$) and direct measures ($Exp.^{B_0}$). All constants are given in GPa.

	C_{11}			C_{12}			C_{44}			B_0			
	PBE	HSE_α	Exp.	PBE	HSE_α	Exp.	PBE	HSE_α	Exp.	PBE	HSE_α	$Exp.^{C_{ij}}$	$Exp.^{B_0}$
AlN	283.1	308.1	…	149.8	161.6	…	179.2	197.2	…	194.2	210.5	…	…
AlP	125.8	133.6	141[a]	61.3	65.1	62[a]	60.8	64.1	70[a]	82.8	87.9	88.3	…
AlAs	103.9	122.1	122[a]	49.1	58.5	57[a]	51.1	59.0	60[a]	67.4	79.7	78.7	74[b]
AlSb	77.0	93.7	88[a]	35.8	43.2	40[a]	36.8	47.5	43[a]	49.5	60.0	56.0	55.1[c]
GaN	253.3	290.0	…	125.2	149.0	…	146.4	173.9	…	167.9	196.0	…	…
GaP	124.6	150.0	140[a]	56.0	64.3	62[a]	65.2	78.4	70[a]	78.9	92.9	88.0	…
GaAs	98.1	122.0	119[a]	42.1	49.4	53[a]	50.8	65.3	60[a]	60.8	73.6	75.0	…
GaSb	74.6	90.1	88[a]	32.0	35.7	40[a]	35.9	49.0	43[a]	46.2	53.8	56.0	…
InN	159.3	188.7	…	102.0	125.8	…	78.9	93.3	…	121.1	146.8	…	…
InP	87.4	105.9	101[d]	45.9	56.4	56[d]	41.9	49.3	46[d]	59.7	72.9	71.0	…
InAs	70.9	91.5	83[a]	37.8	48.8	45[a]	33.1	42.4	40[a]	48.8	62.7	57.6	58[e]
InSb	55.3	74.1	69[a]	29.1	34.8	37[a]	25.4	39.0	31[a]	37.8	47.9	47.7	…
NRMSD (%)	14.3	4.9	…	15.0	5.1	…	13.8	9.2	…	14.4[f]	3.7[f]	…	…

[a]Ultrasound Ref. 77.
[b]X-ray diffraction data from Ref. 9.
[c]Energy dispersive X-ray from Ref. 9.
[d]Ultrasonic-wave transit times Ref. 77.
[e]Ultrasound from Ref. 9.
[f]Comparison with $Exp.^{C_{ij}}$.

investigate the linearity break shown for the III-N compounds, we evaluated the effective Bader charge, as shown in the Table VI in Appendix B. The III-N compounds have a large charge transfer, which indicates that the break in the linearity behavior is due to the high ionicity combined with the smaller atomic radius of the N when compared with the other cations of the III-A column of the Periodic Table. This hypothesis is also supported by the fact that the III-N compounds showed the highest elastic constants values in the series, as discussed in Sec. III C, and the larger observed bond strengths.[76]

C. Elastic constants

The cubic zinc-blende crystal structure has the symmetry defined by the space group $F\bar{4}3m$, which is associated to the point group T_d.[7] The symmetry analysis shows that it possess only three non-equivalent elastic constants: C_{11}, C_{12}, and C_{44}. C_{11} represents the modulus for the axial compression, i.e., the stress in one direction induces a strain in the same direction. In contrast, C_{12} represents the stress that induces a strain in the perpendicular directions, and C_{44}, the shear modulus, represents the strain across the faces induced by the stress in a direction parallel to it. PBE, HSE_α, and the experimental results of C_{11}, C_{12}, and C_{44} are shown in Table II. We also present the bulk modulus, B_0, which was calculated from the expression $B_0 = (C_{11} + 2C_{12})/3$.

Unrelated to the exchange and correlation functionals, the elastic constants in all directions decrease as the ionic radius increases. For the PBE functional, e.g., C_{11} decreases from 283.1 in AlN to 77 in AlSb. The ionic bond character is responsible for the increase on the hardness of the material, and, as shown in the Table VI in Appendix B, the ionicity (related to the Bader charge) decreases as the anion radius decreases. Therefore, it is expected that the elastic constant decreases as the lattice parameter (associated with the cation and anion radii) of the crystal structure increases. In fact, analysis of our results indicates a slight linear dependence with the lattice parameter, as shown in Fig. 3, where the dashed line shows a linear fitting by using all the materials, nitrides excluded. This behavior was reported in the literature[25,78] and was traditionally used to estimate the elastic constants[79,80] by the extrapolation of the data.

In contrast with the lattice parameter overestimation by HSE functionals, the PBE functional underestimates the elastic constants in all the directions, which is consistent with the literature.[81] However, the HSE_α results show better

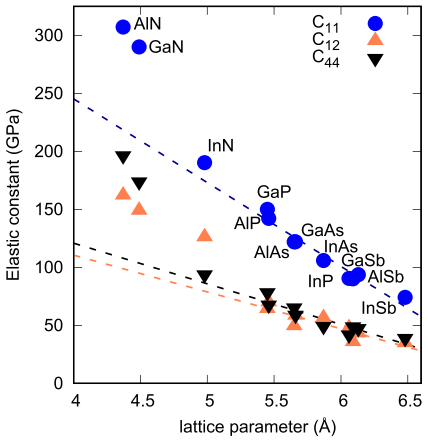

FIG. 3. Dependence of elastic constants on the equilibrium lattice parameter. Elastic constants and lattice parameters have been obtained by using HSE_α functional.

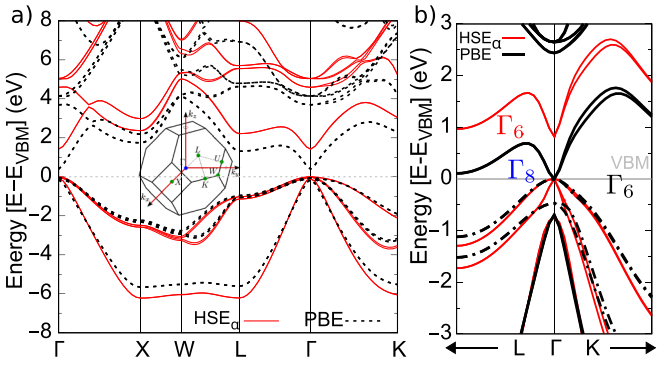

FIG. 4. InP and GaSb band structures evaluated with PBE (dashed line) and HSE$_\alpha$ (solid line), including spin-orbit coupling. (a) band structure for InP. The first Brillouin zone of zinc-blende phase is shown. (b) GaSb band structure close to Γ point: PBE presents a negative band gap, and the HSE$_\alpha$ shows a positive band gap. The band symmetries are indicated.

agreement with the experimental results, which present NRMSDs of 4.9% and 5.1% for C_{11} and C_{12}, respectively. The inclusion of nonlocal effects in the Fock exchange in HSE$_\alpha$ indicates an increasing of the bond hardness, which increases the elastic constants when compared with the PBE functional. For C_{44}, our results, when compared with the experimental data, show deviations for the HSE$_\alpha$ functional similar to the PBE ones when presenting NRMSDs of 13.8% and 9.2%, respectively. Similar C_{44} values were found by Caro *et al.*[82] by using the HSE06 for nitrides. Nonetheless, PBE underestimates the experimental values of C_{11} and C_{12}, whereas HSE$_\alpha$ overestimates them. Because the bulk modulus, B_0, in a cubic system has dependence only in the C_{11} and C_{12} elastic constant directions, the PBE functional also underestimates the B_0 values, whereas the HSE$_\alpha$ functional yields better results. This can be observed by the NRMSD, which is 3.7% and 14.4% for HSE$_\alpha$ and PBE, respectively.

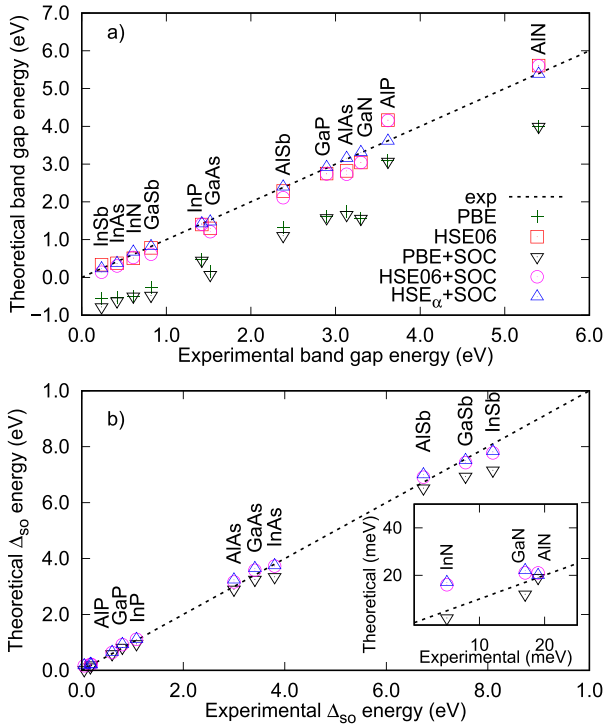

FIG. 5. Energies of the 12 compounds determined with the different functionals with and without the inclusion of the spin-orbit coupling: (a) band gaps (b) spin-orbit splittings. In both figures, the dashed lines show the literature values.

D. Band structures

As discussed previously,[22,24] the PBE functional strongly underestimates the band gap energy. In the specific case of the small band gap III-V materials, its application results in null band gaps or even in the inversion of the ordering of Γ_6 and Γ_8 states, as shown in Fig. 4(b). This

TABLE III. Band gap, $E_{gap} = \Gamma_6^c - \Gamma_8^v$, and spin-orbit splitting, $\Delta_{so} = \Gamma_8^v - \Gamma_7^v$, energies by using the different functionals: PBE, PBE+SOC, HSE06, HSE06+SOC, and HSE$_\alpha$+SOC. The contribution of nonlocal exchange in the HSE, α, adjusted to obtain the experimental values of gap energy and spin-orbit splitting is also shown. The energies are given in eV.

		PBE	PBE+SOC		HSE06	HSE06+SOC		HSE$_\alpha$+SOC		Literature	
	α	E_{gap}	E_{gap}	Δ_{so}	E_{gap}	E_{gap}	Δ_{so}	E_{gap}	Δ_{so}	E_{gap}	Δ_{so}
AlN	0.219	4.003	3.997	0.019	5.609	5.601	0.021	5.383	0.022	5.40[a]	0.019[a]
AlP	0.127	3.090	3.070	0.059	4.164	4.153	0.064	3.611	0.061	3.62[b]	0.06[c]
AlAs	0.343	1.757	1.662	0.290	2.819	2.732	0.316	3.157	0.324	3.13[b]	0.3[b]
AlSb	0.318	1.314	1.105	0.652	2.286	2.111	0.691	2.397	0.700	2.38[b]	0.673[b]
GaN	0.293	1.564	1.560	0.012	3.043	3.042	0.021	3.312	0.022	3.30[d]	0.017[a]
GaP	0.283	1.603	1.576	0.082	2.748	2.739	0.092	2.915	0.093	2.895[b]	0.08[a]
GaAs	0.318	0.166	0.072	0.325	1.297	1.210	0.358	1.471	0.365	1.519[b]	0.341[b]
GaSb	0.297	−0.259	−0.477	0.694	0.782	0.614	0.743	0.819	0.751	0.82[b]	0.756[b]
InN	0.274	−0.504	−0.497	0.002	0.507	0.530	0.016	0.674	0.017	0.61[e]	0.005[a]
InP	0.253	0.468	0.452	0.095	1.402	1.408	0.111	1.422	0.111	1.42[b]	0.108[b]
InAs	0.289	−0.525	−0.626	0.335	0.372	0.301	0.373	0.373	0.385	0.418[b]	0.38[b]
InSb	0.277	−0.558	−0.782	0.716	0.335	0.136	0.778	0.232	0.783	0.235[b]	0.81[b]
NRMSD (%)		55.7	59.1	12.0	9.1	10.9	4.8	1.3	5.4		

[a]Theory from Ref. 40.
[b]Exp. from Ref. 9.
[c]Theory GW from Ref. 83.
[d]Exp. from Ref. 84.
[e]Exp. from Ref. 85.

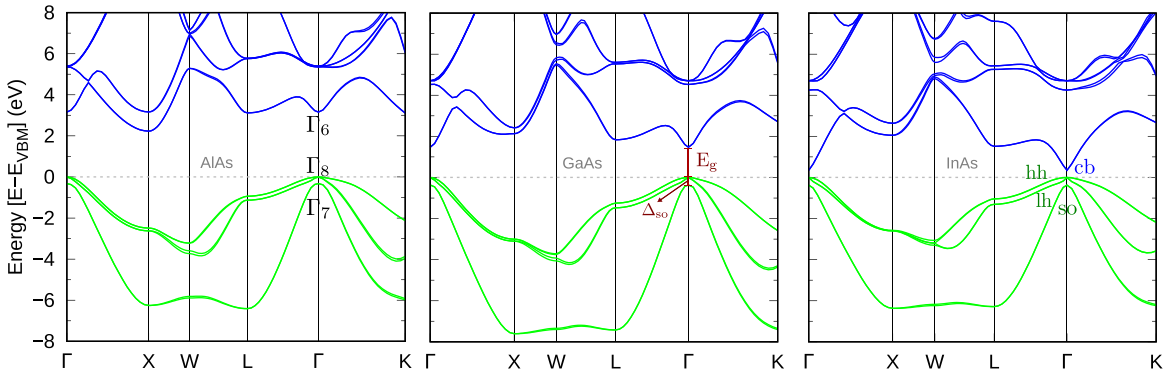

FIG. 6. Band structures obtained by using HSE$_\alpha$+SOC along high symmetry lines for AlAs, GaAs, and InAs. The blue lines indicate conduction bands, whereas the green lines indicate the valence bands. The band structures for the other III-V materials are shown in the supplementary materials.

result is completely inconsistent with the experimental data.[9,40] To get rid of this problem, we used the HSE06 and HSE$_\alpha$ exchange and correlation functions. The differences in the results when using the different functionals may be clarified by analyzing the results, as shown in Fig. 4. The HSE06 and HSE$_\alpha$ gaps are closer to the experimental values than PBE predictions, e.g., InP shows an increase in the value of 68% from PBE to HSE$_\alpha$. An even more dramatic example is the wrong prediction of negative band gaps for InSb, GaSb, InAs, and InN made by using the PBE functional. HSE06 or HSE$_\alpha$ functionals show the correct trend.

Although both HSE06 or HSE$_\alpha$ functionals predict the correct trend, the tuning of α provides a much better agreement for the band gap value, when changing the deviations from the experimental results from 0.8% (InP) up to 42.1% (InSb) when using HSE06 to 0.3% (AlN) and 10.5% (InN) with HSE$_\alpha$. The accuracy in the description of Δ_{so} is also improved when using the hybrid functionals instead of PBE, as shown in Table III. The band structures for all the other materials are presented in the supplementary material.

Regardless of the gap adjustment, i.e., by using the HSE06 calculations, one can notice a monotonic relation between the anionic radius and the band gap energies; e.g., in Al compounds, we observe that $E_{gap}^{AlN} > E_{gap}^{AlP} > E_{gap}^{AlAs} > E_{gap}^{AlSb}$. This trend is also valid for the As compounds, as shown in Fig. 6. It fails, however, for the In compounds, in which the calculated InN band gap is smaller than the trend indicates as shown in Fig. 5. Carrier and Wei[86] indicated, when this same rule was violated for wurtzite compounds, that this was due to the high electronegativity of N and the smaller band gap deformation potentials. In our understanding, the same explanation should be applied to the zinc-blende case (Fig. 6).

E. k · *p* parameters

Despite the fact that band gaps and Δ_{so} are close to the experimental values, there is no guarantee that the calculated band structures are in agreement with the experimental results. To perform this analysis, we calculated the effective masses by using the $\mathbf{k}\cdot p$ approach. In the $\mathbf{k}\cdot p$ method, the interactions that involve electrons and nuclei are described through an effective potential with the same periodicity of the lattice, which allows the utilization of the Bloch's theorem. To find an effective Hamiltonian, we used the perturbative technique proposed by Löwdin,[87] where the basis set is divided in two classes: A and B. States within class A are the states of interest and are described exactly, whereas states from class B are taken into account perturbatively through

TABLE IV. Kane and Luttinger-Kohn parameters obtained through the fitting of the Kane $\mathbf{k}\cdot p$ Hamiltonian in the band structure obtained by using HSE$_\alpha$+SOC close to the Γ point. A range of Luttinger-Kohn parameters found in the compilation of the literature in Refs. 40, 53, and 94 is given for comparison. The $\tilde{\gamma}_s$, γ_s, $\tilde{e}$, and e values are in $\hbar^2/2m_0$ units, whereas E_p values are in eV.

	Kane					Luttinger-Kohn				Range in literature for Luttinger-Kohn parameters				
	$\tilde{\gamma}_1$	$\tilde{\gamma}_2$	$\tilde{\gamma}_3$	$\tilde{e}$	E_P	γ_1	γ_2	γ_3	e	γ_1	γ_2	γ_3	e	E_P
AlN	0.36	−0.20	0.06	−0.10	18.8	1.52	0.38	0.64	3.38	1.92	0.47	0.85	3.03–4.0	27.1
AlP	0.81	−0.48	0.09	−1.01	22.1	2.85	0.54	1.11	5.07	3.35–3.47	0.06–0.71	1.15–1.19	4.55	17.7
AlAs	0.95	−0.61	0.06	−1.26	27.2	3.79	0.92	1.50	6.99	3.25–4.04	0.65–0.9	1.21–1.38	6.67	21.1
AlSb	0.89	−1.05	−0.11	−3.66	27.9	5.02	1.15	1.95	7.88	4.15–5.18	1.01–1.19	1.71–1.81	3.03–8.33	18.7
GaN	0.68	−0.28	0.08	−0.27	16.4	2.39	0.60	0.94	4.87	2.67–3.07	0.75–0.86	1.1–1.16	6.67	25
GaP	1.38	−0.62	0.16	−1.67	25.2	4.20	0.87	1.58	6.68	4.05–4.2	0.49–0.98	1.25–1.95	7.69–10.81	31.4
GaAs	1.37	−0.81	0.10	−2.02	25.9	7.10	2.15	2.99	14.05	6.8–7.8	2.02–2.50	1.0–2.43	14.93–15.43	25.9–27.6
GaSb	1.74	−1.15	0.15	−3.23	24.8	11.78	3.87	5.19	22.04	11.08–13.4	4.03–4.7	5.26–5.74	24.27–25.64	23.7–25.1
InN	0.65	−0.25	0.05	−0.16	11.1	6.13	2.49	2.79	16.15	3.72	1.26	1.63	8.33–14.29	17.2–21.1
InP	1.23	−0.54	0.14	−1.18	18.3	5.33	1.58	2.20	10.86	4.95–6.28	0.94–2.08	1.62–2.08	12.38–14.71	18.1–19.6
InAs	1.29	−0.77	0.10	−1.38	18.9	18.20	7.69	8.55	40.75	19.67–20.5	8.30–8.50	9.10–9.17	37.74–45.66	21.5–21.9
InSb	1.68	−1.04	0.12	−2.09	20.4	31.05	13.65	14.80	63.37	34.5–37.1	14.5–16.5	15.7–17.7	68.49–84.75	23.1–23.5

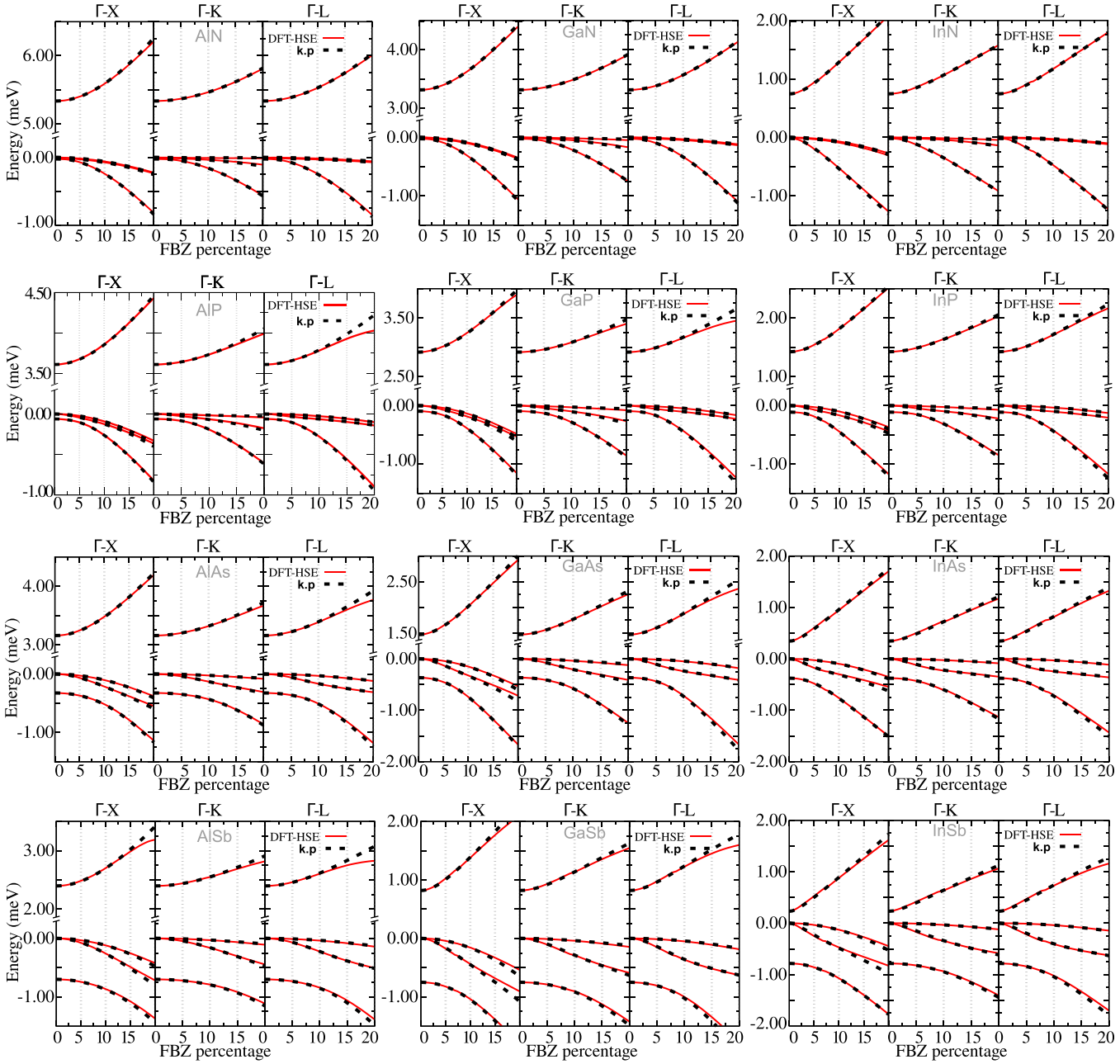

FIG. 7. HSE_α and $\mathbf{k}\cdot p$ band structure comparisons. The optimal parameters were obtained from fitting by using 10% of the FBZ. Three high symmetry directions are shown: Γ-X, Γ-K, and Γ-L.

the interactions with the states of class A. Class A states are chosen according to the energy range at the point of the first Brillouin zone (FBZ), with the goal of defining the effective Hamiltonian.

In this work, we used the 6×6 zinc-blende effective $\mathbf{k}\cdot p$ Hamiltonians proposed by Luttinger and Kohn[88] (LK6) and extended by Kane[89] to an 8×8 model. In the LK6 model, in the vicinity of the Γ point, class A is composed of the three topmost valence bands (VB), i.e., heavy hole (HH), light hole (LH), and spin-orbit split-off hole (SO), and the matrix elements are determined by using the perturbation theory up to the second order. In the Kane model, the same bands and perturbative order were used, but class A also includes the first conduction band (CB). The use the symmetry properties of zinc-blende crystals and some algebraic manipulation[8,90] shows that the Kane Hamiltonian depend on 5 different effective mass parameters $\tilde{\gamma}_1$, $\tilde{\gamma}_2$, $\tilde{\gamma}_3$, $\tilde{e}$, and P, plus the gap and $\Delta_{so,}$ whereas the LK6 depends only on 3 parameters, γ_1, γ_2, and γ_3, plus the $\Delta_{so.}$[91] Because the $\mathbf{k}\cdot p$ method is semi-empirical, all effective mass parameters are obtained, with little algebraic manipulations, from the direct measurements of the effective masses of the carriers in the materials, except for the P parameter.

Distinct from the other effective mass parameters, P cannot be obtained by direct measures but must be extracted from the interband (CB-VB) interaction energy E_P. An accurate measure of E_P is hard to obtain due to the inherent difficulties associated with the decoupling of the CB-VB interaction to the interaction of them with the remote bands. E_P values have been estimated indirectly by experimental

techniques such as electron-spin-resonance, through interband matrix elements[92,93] and from measures of the g-factors, which have little influence from the remote bands and yield more accurate values.[40] Due to the difficulties involved in measuring the g-factor in III-V semiconductors, the traditional procedure is to obtain the P parameter from the effective mass parameters by using the 6×6 $\mathbf{k} \cdot p$ Hamiltonian. When the P is determined, the 8×8 parameters can be evaluated by using the relations shown in Appendix A.

We chose, in this work, an alternative method to determine the effective mass and P parameters from band structures evaluated by DFT calculations. We fitted the HSE_α band structure by using the secular equation of the 8×8 Hamiltonian proposed in Ref. 36, by simultaneously determining all the parameters. All the points have the same weight and the same distance for all the materials. By using different percentages of the FBZ around the Γ point, we determined different parameter sets, and the choice of the final set of parameters was done by root mean square deviation (RMSD) analysis[36] by using the euclidean distance between the band structures from HSE_α and the effective Hamiltonian $\mathbf{k} \cdot p$ with the adjusted parameters. Technical details about the fitting are available in the supplementary material.

As the difference between $\mathbf{k} \cdot p$ and HSE_α increases considerably for large FBZ percentages, we recommend the values from the fitting for 10%, as shown in Table IV. This choice is a compromise between describing a reasonable percentage of the band and obtaining a small deviation of HSE_α band structure. A general feature of the band structures is the non-parabolicity in the region between 6 and 8% of the FBZ, better seen on CB and SO bands, as shown in Fig. 7. Another non-parabolicity also arises near 15%, and depending on the magnitude of this second non-parabolicity in a specific direction, the deviations of the values become more or less important at 20% of the FBZ.

In Table IV, we show the values for Kane ($\tilde{\gamma}_1$, $\tilde{\gamma}_2$, $\tilde{\gamma}_3$, $\tilde{e}$, and E_P), and Luttinger-Kohn (γ_1, γ_2, γ_3, and e) parameters, determined with the data by using the range of up to 10% of the FBZ (and in any up to a range of 2% to 20% in the supplementary materials). The ranges of the values observed in the literature are also given for comparison. Due to the small number of results founded in the literature, we included both experimental and theoretical works, which indicate the maximum and minimum values extracted from traditional sources, such as Madelung *et al.*,[53] Vurgaftman *et al.*,[40] , Vurgaftman and Meyer,[94] and Winkler.[95] Our results are in agreement with the literature, i.e., the obtained effective mass parameters are inside the range of the most accepted values. In addition, the highest deviation comes from the nitrides. Because the most stable phase for the III-nitrides is wurtzite and not zinc-blende, the scarce experimental data prevents a more controlled comparison.

On the Kane models, the P parameter, or its related energy E_P, is essential. This parameter represents the influence of the conduction band on the masses of the valence states and, consequently, the influence of the valence band on the conduction states. Our results for the E_P parameter differ from those in the literature. The main reason for this difference is a divergence on the interpretation of the influence of the remote bands on the experimental measurements of the electron spin resonance as pointed out by Shantharama *et al.*[96] and Adams *et al.*[97] In their article they compare, e.g., Chadi *et al.*, [93] the value for GaAs of $E_P = 29$ eV, with their estimation based on an analysis of a 14×14 $\mathbf{k} \cdot p$ Hamiltonian of $E_P = 25 \pm 0.5$ eV. The reason for the divergence is atributed to an overestimation of the influence of the remote bands. Our suggested value for this parameter is $E_P = 25.9$ eV. Because E_P is directly related to the Kane parameter P, its fitting is essential.

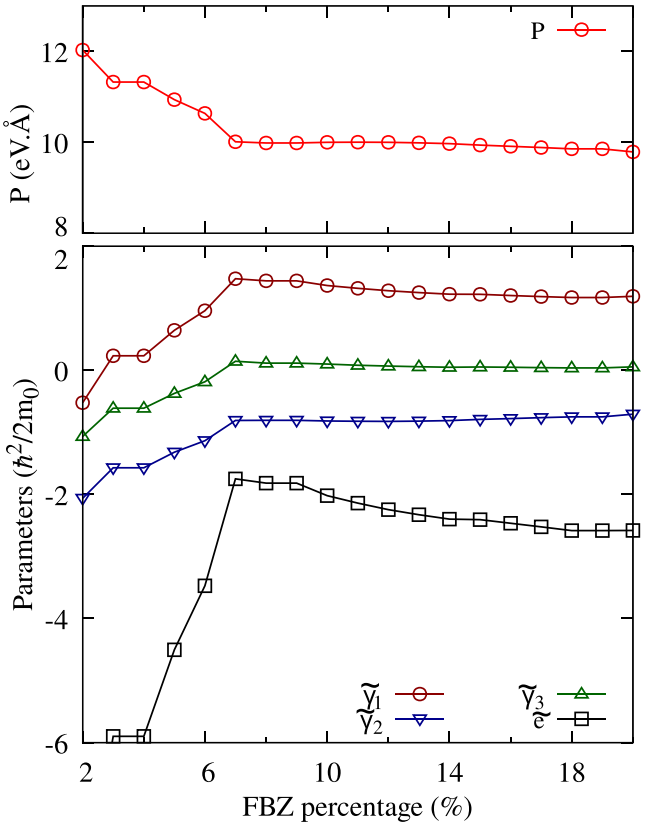

FIG. 8. GaAs dependence of P and Kane parameters with FBZ region used in the fitting process.

As we previously showeded,[36] to correctly assign a value to P, it is necessary to include the first non-parabolicity in the range used for the fitting. If only the values below it are included, then there is a fast variation of the values of P, depending on the range used. However, the fittings done with ranges, including the non-parabolicity, show a stabilization of the value. As an example, in Fig. 8, we present a curve of the fitted parameter for GaAs, which shows the fast variation for ranges very close to the Γ-point and the stabilized values for ranges above 8%. The stabilization of our values indicates that our method improves the evaluation of the P parameter, which provides a way to distinguish the interactions of near and distant bands in the effective mass tensor. In the supplementary materials, we provide the stabilization curves for the P as well as the effective mass parameters for all the materials.

F. Effective mass and *g*-factors

To verify the accuracy of our calculations, we compared the experimental effective masses with the ones obtained

TABLE V. Effective masses for light and the heavy holes along three directions ([100], [110], and [111]), isotropic masses from conduction band electrons and spin-orbit splitting holes, and electron g-factors, obtained around the Γ point, from the Luttinger-Kohn parameters. The ranges of values that comprise the values found in the literature (experimental and theoretical results) are also shown for comparison.

		[100]		[110]		[111]				
		m^*_{HH}	m^*_{LH}	m^*_{HH}	m^*_{LH}	m^*_{HH}	m^*_{LH}	m^*_{so}	m^*_e	g^*_c
AlN	This work	1.320	0.437	4.123	0.357	2.858	0.371	0.659	0.296	1.99
	Literature								0.330[a]	
AlP	This work	0.563	0.255	1.599	0.197	1.176	0.206	0.355	0.197	1.93
	Literature	0.513[b]	0.211[b]			1.372[b]	0.145[b]	0.30[a]		
AlAs	This work	0.503	0.177	0.955	0.152	1.253	0.146	0.282	0.143	1.46
	Literature	0.409[c]	0.153[c]			1.022[c]	0.109[c]	0.28[a]	0.15[c]	
AlSb	This work	0.359	0.136	0.682	0.115	0.890	0.111	0.240	0.127	0.20
	Literature	0.336[c]	0.123[c]			0.872[c]	0.091[c]		0.14[a]	
GaN	This work	0.841	0.279	1.542	0.243	1.991	0.234	0.421	0.205	1.98
	Literature									1.95[d]
GaP	This work	0.405	0.168	0.754	0.141	0.966	0.136	0.243	0.150	1.82
	Literature					0.670[c]	0.170[c]	0.465[e]	0.13[a]	
GaAs	This work	0.357	0.088	0.672	0.079	0.898	0.076	0.169	0.071	−0.34
	Literature	0.34[b]	0.094[b]			0.75[b]	0.082[b]		0.0662[b]	−0.44[f]
GaSb	This work	0.247	0.051	0.500	0.046	0.710	0.045	0.144	0.045	−7.66
	Literature	0.29[c]		0.36[c]		0.40[c]		0.12[a]	0.039[b]	−9.1[c]
InN	This work	0.874	0.090	1.851	0.085	1.460	0.086	0.167	0.062	1.73
	Literature									
InP	This work	0.460	0.118	0.828	0.106	1.073	0.103	0.199	0.092	1.38
	Literature							0.121[b]	0.0808[b]	1.48[b]
InAs	This work	0.354	0.030	0.911	0.028	0.661	0.029	0.104	0.025	−15.18
	Literature	0.35[b]				0.85[b]		0.14[a]	0.0265[b]	−15.3[b]
InSb	This work	0.266	0.017	0.498	0.017	0.692	0.016	0.119	0.016	−43.30
	Literature	0.32[c]		0.42[c]		0.44[c]		0.11[a]	0.013[b]	−51.31[b]

[a]Theory from Ref. 40.
[b]Exp. from Ref. 9.
[c]Exp. from Ref. 77.
[d]Exp. from Ref. 85.
[e]Theory from Ref. 77.
[f]Exp. from Ref. 99.

from our effective mass parameters (see relations in Appendix A). By using the electronic g-factors, which are directly related to the spin splitting of the carrier bands, we compared the measured values in the literature with our own values estimated from the $\mathbf{k}\cdot p$ parameters by using the Roth's formula[98]

$$g^*_c = 2 - \frac{2E_p\Delta_{so}}{3E_{gap}(E_{gap}+\Delta_{so})}, \tag{4}$$

and the values for E_P, E_{gap}, and Δ_{so}. This equation includes only the interaction between VB and CB, whereas the interactions between the other bands are neglected.

Table V shows the effective masses and g-factors obtained by the $\mathbf{k}\cdot p$ parameters calculation. SO and CB electronic effective masses are considered to be isotropic, and HH and LH were evaluated along three different directions of the FBZ: [111], [110], and [100]. The CB g-factors were estimated by using Eq. (4). Tabulated values, extracted from Refs. 40, 53, 77, and 94, are presented for comparison. The supplementary material provides tables for all calculated parameter sets.

Because we can distinguish the effects of the interactions from inner and outer bands, our g-factors show excellent agreement with the literature values except those materials with large spin-orbit coupling, such as antimonides and indium compounds. In these materials, we found large deviations from the reference values of HH and LH effective masses along the [110] and [111] directions. The lack of k dependence on the spin-orbit coupling on the $\mathbf{k}\cdot p$ Hamiltonian used in our description may be responsible for such deviation. However, even for these materials, the LH and HH g-factors along the [100] direction present good agreement with the experimental values because the specific symmetry of the zinc-blende systems prevent the splitting of the bands along that specific direction. Finally, CB and SO bands also present good agreement with the experimental values because the spin split for them is small.

IV. SUMMARY AND CONCLUSION

We reported an extensive *ab initio* study of electronic and structural properties of the III-V semiconductors (12 systems) based on DFT within the PBE, PBE+SOC, HSE06, HSE_α, and HSE_α+SOC functionals. For the hybrid HSE_α

functional, we fitted the magnitude of the nonlocal Fock exchange that replaces part of the PBE exchange based on the experimental results for the fundamental band gap and spin-orbit splitting energies. Except for the AlP compound, whose α is 0.127, our α parameters are in between 0.209 and 0.343, deviating less than 0.1 from the universal value of 0.25 estimated by Perdew *et al.*[28]

Although the electronic properties were improved by the fitting, our results and analysis clearly indicate that HSE_α does not yield a significant improvement of the structural properties when compared with HSE06. In fact, it is an excellent result because it shows that it is possible to improve the electronic properties without affecting the structural parameters by using fitted HSE_α functionals. This conclusion is valid at least for small changes in α near to the 0.25 value. Furthermore, based on several analysis, we found a correlation between the values of α with the cationic radius, namely, the optimized α value decreases almost linearly as a function of the atomic cationic radius, except for the case of AlN. Therefore, our findings, combined with previous results obtained by Viñes *et al.*,[34] indicate that it is possible to correlate the values of the α with the physical properties, and, hence, it opens new possibilities in the study of much more complex materials.

We found that the HSE_α overestimates the elastic constants, whereas PBE underestimates them. However, the magnitude of the relative error is smaller when using the HSE_α functional. We see from our results that the elastic constants decrease as the ionic radius increase, and, hence, the elastic constants decrease by increasing the lattice parameter of the crystal structures. This behavior was reported in the literature[25,78] and was traditionally used to estimate the elastic constants[79,80] by the extrapolation of the data.

To provide a deeper understanding of the band structure curvatures, we used the DFT band structures to determine accurate $\mathbf{k}\cdot p$ parameters and, from them, obtained the effective masses and the g-factors beyond the parabolic model. For the antimonides and indium compounds in specific directions, we observed large deviations of the g-factors from the experimental results, which indicate that the 8×8 $\mathbf{k}\cdot p$ Hamiltonian may still not be adequate for describing systems with small band gap or large spin-orbit splittings. The k-dependent spin-orbit term, responsible for the spin-orbit splitting outside of the Γ point, is neglected in our model, which results in the deviations observed. Finally, we tabulated the effective masses and $\mathbf{k}\cdot p$ parameters by presenting a full set of III-V parameters that may be used in realistic simulations of systems with higher complexity, such as nanowires and quantum dots or devices based on these compounds.

SUPPLEMENTARY MATERIAL

See supplementary material for additional data: computational parameters used for every system, analyses of the α parameter versus different physical properties, band structures, and $\mathbf{k}\cdot p$ parameters for different percentages of the BZ for all the systems.

ACKNOWLEDGMENTS

The authors thank D. J. As for the help with experimental data on nitride systems. The authors acknowledge financial support from the Brazilian agencies CAPES, PVE Grant No. 88881.068174/2014-01 (G. M. Sipahi), São Paulo research foundation, Grant No. 2013/21045-2 (J. L. F. Da Silva), national council for scientific and technological development, 301190/2015-1 (J. L. F. Da Silva), and the coordination for improvement of higher level education (C. M. O. Bastos and F. P. Sabino). The authors also thank the infrastructure provided to our computer cluster by the department of information technology, campus São Carlos.

APPENDIX A: EFFECTIVE BADER CHARGE

TABLE VI. Effective Bader charge evaluated by using the PBE functional for III-V semiconductors. All units are in C.

	N	P	As	Sb
Al	2.37	2.06	1.92	1.63
Ga	1.52	0.84	0.68	0.34
In	1.40	0.88	0.74	0.47

APPENDIX B: LUTTINGER–KOHN PARAMETERS AND EFFECTIVE MASS RELATIONS

Because class A and B states differ among the 6×6 and 8×8 models, the definitions of the effective mass parameters differ from one model to the other.[8,90] The relation between both model parameters, for zinc-blende structures, is given by the following expressions:

$$\gamma_1 = \tilde{\gamma}_1 + \frac{E_p}{3E_{gap}}, \quad \gamma_2 = \tilde{\gamma}_2 + \frac{E_p}{6E_{gap}},$$

$$\gamma_3 = \tilde{\gamma}_3 + \frac{E_p}{6E_{gap}}, \quad e = \tilde{e} + \frac{\left(E_{gap} + \frac{2}{3}\Delta_{so}\right)E_p}{E_{gap}(E_{gap}+\Delta_{so})},$$

$$E_p = \frac{2m_0}{\hbar^2}P^2.$$

The effective masses may be determined from the parameters by using the following relations:

$$m_{lh[100]} = (\gamma_1 + 2\gamma_2)^{-1}, \quad m_{lh[110]} = (\gamma_1 + 2\gamma_3)^{-1},$$
$$m_{hh[100]} = (\gamma_1 - 2\gamma_2)^{-1}, \quad m_{hh[110]} = (\gamma_1 - 2\gamma_3)^{-1},$$
$$m_e = e^{-1}, \quad m_{lh[111]} = (\gamma_1 + \sqrt{\gamma_2^2 + 3\gamma_3^2})^{-1},$$
$$m_{hh[111]} = (\gamma_1 - \sqrt{\gamma_2^2 + 3\gamma_3^2})^{-1},$$
$$m_{so} = \left(\gamma_1 - \frac{1}{3}\frac{\Delta_{so}E_p}{E_{gap}(E_{gap}+\Delta_{so})}\right)^{-1}.$$

[1]E. F. Schubert, *Light-Emitting Diodes* (Cambridge University Press, 2006).
[2]S. Nakamura, Rev. Mod. Phys. **87**, 1139 (2015).

[3]Y. Sun, K. Zhou, Q. Sun, J. Liu, M. Feng, Z. Li, Y. Zhou, L. Zhang, D. Li, S. Zhang, M. Ikeda, S. Liu, and H. Yang, Nat. Photonics **10**, 595 (2016).
[4]A. Rogalski, *Infrared Detectors* (CRC Press, 2010).
[5]J. Nelson, *The Physics of Solar Cells* (ICP, 2003).
[6]D. Basu, D. Saha, C. C. Wu, M. Holub, Z. Mi, and P. Bhattacharya, Appl. Phys. Lett. **92**, 091119 (2008).
[7]P. Y. Yu and M. Cardona, *Fundamentals of Semiconductors*, 2nd ed. (Spinger-Verlag, Berlin, 1999).
[8]R. Enderlein, *Fundamentals of Semiconductor Physics and Devices* (World Scientific, 1997).
[9]O. Madelung, *Semiconductors: Data Handbook* (Springer, Berlin/Heidelberg, 2004).
[10]M. Z. Hasan and C. L. Kane, Rev. Mod. Phys. **82**, 3045 (2010).
[11]T. D. Stanescu, R. M. Lutchyn, and S. D. Sarma, Phys. Rev. B **84**, 144522 (2011).
[12]V. Mourik, K. Zuo, S. M. Frolov, S. R. Plissard, E. P. A. M. Bakkers, and L. P. Kouwenhoven, Science **336**, 1003 (2012).
[13]*Liquid Crystalline Semiconductors*, edited by R. J. Bushby, S. M. Kelly, and M. O'Neill (Springer, Netherlands, 2013).
[14]M. Gmitra and J. Fabian, Phys. Rev. B **94**, 165202 (2016).
[15]M. A. T. Sandoval, E. A. de Andrada e Silva, A. F. da Silva, and G. C. La Rocca, Semicond. Sci. Technol. **31**, 115008 (2016).
[16]S. J. Polly, C. G. Bailey, A. J. Grede, D. V. Forbes, and S. M. Hubbard, J. Cryst. Growth **454**, 64 (2016).
[17]M. S. Seghilani, M. Myara, M. Sellahi, L. Legratiet, I. Sagnes, G. Beaudoin, P. Lalanne, and A. Garnache, Sci. Rep. **6**, 38156 (2016).
[18]P. E. Faria Junior, T. Campos, C. M. O. Bastos, M. Gmitra, J. Fabian, and G. M. Sipahi, Phys. Rev. B **93**, 235204 (2016).
[19]C.-Z. Zhao, T. Wei, X.-D. Sun, S.-S. Wang, and K.-Q. Lu, Physica B **494**, 71 (2016).
[20]M. O. Nestoklon, R. Benchamekh, and P. Voisin, J. Phys.: Condens. Matter **28**, 305801 (2016).
[21]J. P. Perdew and A. Zunger, Phys. Rev. B **23**, 5048 (1981).
[22]J. P. Perdew and M. Levy, Phys. Rev. Lett. **51**, 1884 (1983).
[23]R. O. Jones and O. Gunnarsson, Rev. Mod. Phys. **61**, 689 (1989).
[24]Y.-S. Kim, M. Marsman, G. Kresse, F. Tran, and P. Blaha, Phys. Rev. B **82**, 205212 (2010).
[25]S. Adachi, *Physical Properties of III-V Semiconductor Compounds* (Wiley-Blackwell, 1992).
[26]L. Hedin, Phys. Rev. **139**, A796 (1965).
[27]F. Aryasetiawan and O. Gunnarsson, Rep. Prog. Phys. **61**, 237 (1998).
[28]J. P. Perdew, M. Ernzerhof, and K. Burke, J. Chem. Phys. **105**, 9982 (1996).
[29]C. Adamo and V. Barone, J. Chem. Phys. **110**, 6158 (1999).
[30]J. Heyd, G. E. Scuseria, and M. Ernzerhof, J. Chem. Phys. **118**, 8207 (2003).
[31]J. Heyd and G. E. Scuseria, J. Chem. Phys. **121**, 1187 (2004).
[32]J. Heyd, G. E. Scuseria, and M. Ernzerhof, J. Chem. Phys. **124**, 219906 (2006).
[33]A. D. Becke, J. Chem. Phys. **98**, 5648 (1993).
[34]F. Viñes, O. Lamiel-García, K. C. Ko, J. Y. Lee, and F. Illas, J. Comput. Chem. **38**, 781 (2017).
[35]P. G. Moses, M. Miao, Q. Yan, and C. G. Van de Walle, J. Chem. Phys. **134**, 084703 (2011).
[36]C. M. O. Bastos, F. P. Sabino, P. E. F. Junior, T. Campos, J. L. F. Da Silva, and G. M. Sipahi, Semicond. Sci. Technol. **31**, 105002 (2016).
[37]L. E. Ramos, L. K. Teles, L. M. R. Scolfaro, J. L. P. Castineira, A. L. Rosa, and J. R. Leite, Phys. Rev. B **63**, 165210 (2001).
[38]A. Dal Corso, Phys. Rev. B **86**, 085135 (2012).
[39]J. Paier, M. Marsman, K. Hummer, G. Kresse, I. C. Gerber, and J. G. Ángyán, J. Chem. Phys. **124**, 154709 (2006).
[40]I. Vurgaftman, J. R. Meyer, and L. R. Ram-Mohan, J. Appl. Phys. **89**, 5815 (2001).
[41]P. Hohenberg and W. Kohn, Phys. Rev. **136**, B864 (1964).
[42]W. Kohn and L. J. Sham, Phys. Rev. **140**, A1133 (1965).
[43]J. P. Perdew and Y. Wang, Phys. Rev. B **45**, 13244 (1992).
[44]J. P. Perdew, J. A. Chevary, S. H. Vosko, K. A. Jackson, M. R. Pederson, D. J. Singh, and C. Fiolhais, Phys. Rev. B **46**, 6671 (1992).
[45]J. P. Perdew, K. Burke, and M. Ernzerhof, Phys. Rev. Lett. **77**, 3865 (1996).
[46]M. Ernzerhof and G. E. Scuseria, J. Chem. Phys. **110**, 5029 (1999).
[47]J. L. F. Da Silva, M. V. Ganduglia-Pirovano, J. Sauer, V. Bayer, and G. Kresse, Phys. Rev. B **75**, 045121 (2007).
[48]M. V. Ganduglia-Pirovano, J. L. F. Da Silva, and J. Sauer, Phys. Rev. Lett. **102**, 026101 (2009).
[49]Y. Hinuma, A. Grüneis, G. Kresse, and F. Oba, Phys. Rev. B **90**, 155405 (2014).
[50]A. V. Krukau, O. A. Vydrov, A. F. Izmaylov, and G. E. Scuseria, J. Chem. Phys. **125**, 224106 (2006).
[51]D. D. Koelling and B. N. Harmon, J. Phys. C: Solid State Phys. **10**, 3107 (1977).
[52]T. Takeda, Z. Phys. B **32**, 43 (1978).
[53]*Semiconductors: Physics of Group IV Elements and III-V Compounds*, Landolt-Börnstein, New Series, Group III Vol. 17, editedby O. Madelung, M. Schultz, and H. Weiss (Springer-Verlag, Berlin, 1982).
[54]P. E. Blöchl, Phys. Rev. B **50**, 17953 (1994).
[55]G. Kresse and J. Hafner, Phys. Rev. B **48**, 13115 (1993).
[56]G. Kresse and J. Furthmüller, Phys. Rev. B **54**, 11169 (1996).
[57]G. Kresse and D. Joubert, Phys. Rev. B **59**, 1758 (1999).
[58]Y. L. Page and P. Saxe, Phys. Rev. B **65**, 104104 (2002).
[59]X. Wu, D. Vanderbilt, and D. R. Hamann, Phys. Rev. B **72**, 035105 (2005).
[60]J. Heyd, J. E. Peralta, G. E. Scuseria, and R. L. Martin, J. Chem. Phys. **123**, 174101 (2005).
[61]Y.-S. Kim, K. Hummer, and G. Kresse, Phys. Rev. B **80**, 035203 (2009).
[62]J. P. Perdew, W. Yang, K. Burke, Z. Yang, E. K. U. Gross, M. Scheffler, G. E. Scuseria, T. M. Henderson, I. Y. Zhang, A. Ruzsinszky, H. Peng, J. Sun, E. Trushin, and A. Görling, Proc. Natl. Acad. Sci. U. S. A. **114**, 2801 (2017).
[63]V. Atalla, I. Y. Zhang, O. T. Hofmann, X. Ren, P. Rinke, and M. Scheffler, Phys. Rev. B **94**, 035140 (2016).
[64]N. Sai, P. F. Barbara, and K. Leung, Phys. Rev. Lett. **106**, 226403 (2011).
[65]W. Yang, A. J. Cohen, and P. Mori-Sánchez, J. Chem. Phys. **136**, 204111 (2012).
[66]A. Walsh, J. L. F. Da Silva, and S.-H. Wei, Phys. Rev. Lett. **100**, 256401 (2008).
[67]H.-P. Komsa and A. Pasquarello, Phys. Rev. B **84**, 075207 (2011).
[68]D. Colleoni and A. Pasquarello, J. Phys.: Condens. Matter **28**, 495801 (2016).
[69]R. Todeschini, V. Consonni, R. Mannhold, H. Kubinyi, and G. Folkers, *Molecular Descriptors for Chemoinformatics* (Wiley VCH Verlag GmbH, 2009), Vol. 41.
[70]J. C. Slater, J. Chem. Phys. **41**, 3199 (1964).
[71]C. Kittel, *Introduction to Solid State Physics*, 8th ed. (John Wiley & Sons, Inc., New York, 2004).
[72]H. Morkoç, *Handbook of Nitride Semiconductors and Devices, Materials Properties, Physics and Growth* (John Wiley & Sons, 2009), Vol. 1.
[73]S. J. Pearton, *GaN and Related Materials II (Optoelectronic Properties of Semiconductors and Superlattice)* (CRC Press, 2000), Vol. 2.
[74]*New Data and Updates for IV-IV, III-V, II-VI and I-VII Compounds, Their Mixed Crystals and Diluted Magnetic Semiconductors*, edited by U. Rössler (Springer, Berlin/Heidelberg, 2011).
[75]N. N. Anua, R. Ahmed, A. Shaari, M. A. Saeed, B. U. Haq, and S. Goumri-Said, Semicond. Sci. Technol. **28**, 105015 (2013).
[76]*Introduction to Nitride Semiconductor Blue Lasers and Light Emitting Diodes*, edited by S. Nakamura and S. F. Chichibu (CRC Press, 2000).
[77]*Springer Handbook of Condensed Matter and Materials Data*, edited by W. Martienssen and H. Warlimont (Springer Nature, 2005).
[78]R. W. Keyes, J. Appl. Phys. **33**, 3371 (1962).
[79]*Semiconductors and Semimetals: Transport Phenomena*, edited by R. K. Willardson and A. C. Beer (Academic Press Inc., 1975), Vol. 10.
[80]S. Adachi, J. Appl. Phys. **58**, R1 (1985).
[81]M. Łopuszyński and J. A. Majewski, Phys. Rev. B **76**, 045202 (2007).
[82]M. A. Caro, S. Schulz, and E. P. O'Reilly, Phys. Rev. B **86**, 014117 (2012).
[83]A. N. Chantis, M. van Schilfgaarde, and T. Kotani, Phys. Rev. Lett. **96**, 086405 (2006).
[84]B. Monemar, Phys. Rev. B **10**, 676 (1974).
[85]J. H. Buß, T. Schupp, D. J. As, D. Hägele, and J. Rudolph, J. Appl. Phys. **118**, 225701 (2015).
[86]P. Carrier and S.-H. Wei, J. Appl. Phys. **97**, 033707 (2005).
[87]P.-O. Löwdin, J. Chem. Phys. **19**, 1396 (1951).
[88]J. M. Luttinger and W. Kohn, Phys. Rev. **97**, 869 (1955).
[89]E. O. Kane, *Semiconductors and Semimetals* (Elsevier BV, 1966), pp. 75–100.
[90]M. W. Lok and C. Lew Yan Voon, *The **k.p** Method* (Springer-Verlag GmbH, 2009).

[91]We denoted the 6×6 parameters, the so called Luttinger-Kohn parameters without tilde. In opposition, the 8×8 ones are referred as Kane parameters.
[92]C. Weisbuch and C. Hermann, Phys. Rev. B **15**, 816 (1977).
[93]D. J. Chadi, A. H. Clark, and R. D. Burnham, Phys. Rev. B **13**, 4466 (1976).
[94]I. Vurgaftman and J. R. Meyer, J. Appl. Phys. **94**, 3675 (2003).
[95]R. Winkler, *Spin-Orbit Coupling Effects in Two-Dimensional Electron and Hole Systems* (Springer-Verlag, Berlin, 2003).
[96]L. G. Shantharama, A. R. Adams, C. N. Ahmad, and R. J. Nicholas, J. Phys. C: Solid State Phys. **17**, 4429 (1984).
[97]A. R. Adams, L. G. Shantharama, R. J. Nicholas, and C. K. Sarkar, Physica B **139–140**, 401 (1986).
[98]L. M. Roth, B. Lax, and S. Zwerdling, Phys. Rev. **114**, 90 (1959).
[99]M. Oestreich and W. W. Rühle, Phys. Rev. Lett. **74**, 2315 (1995).